Predicting Spectral Halftone Measurements for Different Instruments Using a New Multi-Scale Approach

Milos Sormaz*, Safer Mourad**, Tobias Stamm**, Patrick Jenny*
Swiss Federal Institute of Technology (ETH), Institute of Fluid Dynamics, Zürich, Switzerland
****Swiss Federal Laboratory for Materials Testing and Research (EMPA), Laboratory for Media Technology, Dübendorf, Switzerland***

Abstract

The objective of this work is to predict the deviations between spectral measurements obtained by different devices for halftone prints. To describe the physics, the transport theory is considered, and to accurately solve the governing equations for arbitrary phase functions, a stochastic Monte Carlo method is employed. Recently, a stencil approach was developed, which allows to speed up such Monte Carlo algorithms significantly without compromising their accuracy. However, even with the stencil method the computational cost of well resolved simulations becomes exorbitant, if large halftone patches with huge numbers of individual dots are considered. To overcome this problem, a new multi-scale algorithm is devised. For large samples with statistically homogeneous dot patterns, it allows an additional increase of the efficiency without affecting the accuracy. In our studies we compare measurements of print patches captured with a hand-held eye one device and a microscopic spectrophotometer. Varying illumination and capturing geometries throughout different measuring devices pose a challenge to accurately predict the measurement differences with numerical models. These geometries were determined and implemented as boundary conditions of the simulated domains. Evaluations are presented that demonstrate reasonable agreement between the computed and the experimental data for ten halftone samples with ergodic, isotropic halftone patterns of different ink coverage.

Introduction

Using different color measuring devices and comparing the readouts of the instruments poses a common challenge in graphic arts industry. It is quite common to obtain spectral deviations between the instruments with a magnitude of about 10%. This value is even exceeded in our particular case of interest, where we aim at comparing the readouts obtained from a microspectrophotometer with the values of a hand-held macroscopic device such as an *eye one™(i1)* or others (Fig. 1). In this paper we propose a method for transforming spectral microscopic observations into spectral predictions of common macroscopic measurements. In spectral calculations, the prediction problem for perfectly diffuse (isotropic, lambertian) reflectors reduces to the easy case of considering the various radiation geometries within both instruments and to account for their deviations by using an adjusting geometric factor [9]. However, the prevalent materials in graphic arts are apart from being perfectly diffusing, a fact which explains the difficulties in comparing the readouts obtained. We tackle this challenge by accounting for the significant geometric parameters of both measurement setups (see Fig. 2) and by using an enhanced numerical simulation approach that allows for the departure of the radiation's angular distribution from the lambertian case.

The model used for the simulations is based on the transport theory [1]. Similar to classical Monte Carlo methods [2], computational particles are transported through the domain. In order to improve the computational efficiency, a previously developed stencil approach [3] is employed. Efficiency and accuracy of this stencil method were demonstrated in previous works [4].

For the scenarios considered here, this stencil approach is extended for paper substrates with magenta ink patterns and in order to deal with halftone samples containing large numbers of dots, a multi-scale method was devised. For the class of problems considered here, this general statistical modeling approach introduces no additional assumptions or simplifications. We considered ten patches of different ink coverage, for which the numerical results are compared with measurements of both devices, the hand-held i1 and the microscope.

Computational Approach

As already mentioned, the transport theory [1] is considered for the description of light propagation, scattering and absorption. The basic governing equation reads

$$\frac{dI(\boldsymbol{x},\boldsymbol{s})}{ds} = -\gamma_t I(\boldsymbol{x},\boldsymbol{s}) + \frac{\gamma_s}{4\pi}\int_{4\pi} p(\boldsymbol{s},\tilde{\boldsymbol{s}}) I(\boldsymbol{x},\tilde{\boldsymbol{s}}) d\tilde{\omega} \qquad (1)$$

with $\gamma_t = \gamma_s + \gamma_a$ and describes the change of the radiance $I(\boldsymbol{x},\boldsymbol{s})$ along the propagation direction $\boldsymbol{s}$. The first term on the right-hand side describes losses for that direction due to absorption and scattering, where γ_a and γ_s are absorption and scattering coefficients, respectively. The light scattered from all other directions $\tilde{\boldsymbol{s}}$ to direction $\boldsymbol{s}$ is accounted for by the last term, where $p(\boldsymbol{s},\tilde{\boldsymbol{s}})$ is the phase function with

$$\int_{4\pi} p(\boldsymbol{s},\tilde{\boldsymbol{s}}) d\tilde{\omega} \equiv 1. \qquad (2)$$

Note that the radiance is a function of $\boldsymbol{x}$ and $\boldsymbol{s}$ and can be interpreted as a mass density function, i.e. as the product of the probability density function $f(\boldsymbol{s};\boldsymbol{x})$ and the radiant energy fluence rate

$$\Psi(\boldsymbol{x}) = \int_{4\pi} I(\boldsymbol{x},\boldsymbol{s}) d\omega. \qquad (3)$$

In Monte Carlo methods [2], this mass density function is represented as a cloud of many computational particles, each having a position $\hat{\boldsymbol{x}}$ and a propagation direction $\hat{\boldsymbol{s}}$. Consistent evolution of a particle is achieved by determining first a random variable, which quantifies the time Δt_s till the next scattering event. It is exponentially distributed and its mean value is $\tau_s = 1/(c\gamma_s)$ with the speed of light c. The new particle position then becomes $\hat{\boldsymbol{x}} + c\hat{\boldsymbol{s}}\Delta t_s$ and the new propagation direction after the scattering event is calculated based on a second random number with a distribution consistent with the phase function. Moreover, the mass of the particle, which represents its associated energy $\hat{e}_p$, decreases by the amount $\Delta\hat{e}_p = (1 - e^{-c\gamma_a\Delta t_s})\hat{e}_p$. Especially for substrate thicknesses $d \gg 1/\gamma_s$, such Monte Carlo

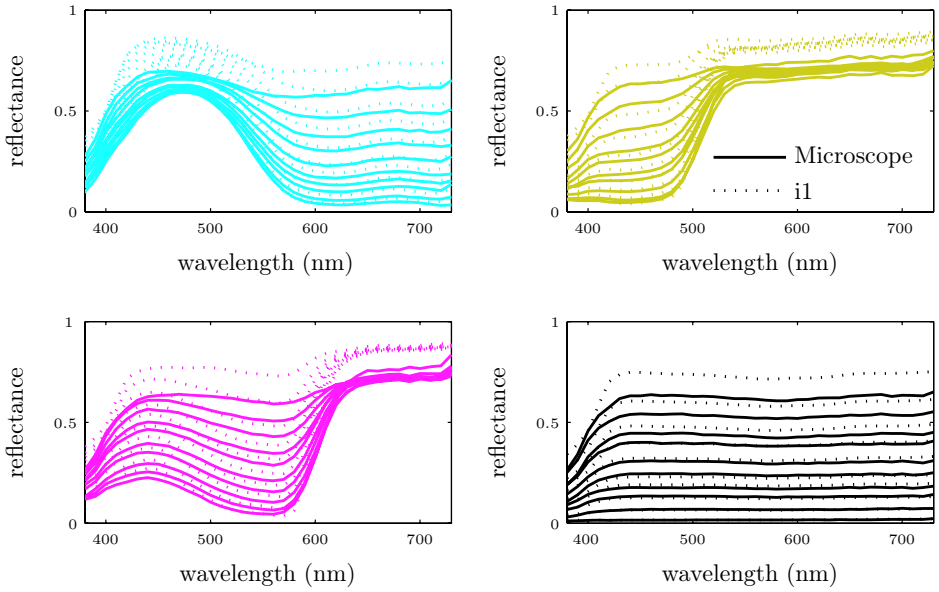

Figure 1. *Spectral comparison between microscope and i1 measurements.*

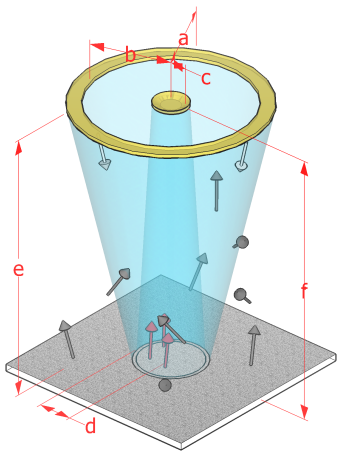

Figure 2. *Sketch of the illumination and sensor geometries used by the measuring devices.*

methods become expensive since many time steps are required for a particle to pass through the substrate. This was the motivation for a recently developed stencil method [3, 4], which is as accurate as the stochastic Monte Carlo approach, but proved to be much more efficient in cases with $d \gg 1/\gamma_s$, if relatively large homogeneous regions can be identified within the substrate.

Stencil Method

The stencil method can be applied within homogeneous patches, where synchronous time stepping for the particle evolution is employed. Each time step of size Δt, the joint statistics of the particle dislocations $\Delta\hat{\boldsymbol{x}} = \hat{\boldsymbol{x}}(t+\Delta t) - \hat{\boldsymbol{x}}(t)$ and the new propagation directions $\hat{\boldsymbol{s}}(t+\Delta t)$ is obtained from transformed table entries. The tables store the results of small Monte Carlo simulations lasting for the duration Δt. For these a-priory simulations the scattering coefficients and the phase functions of the corresponding patches are employed, and a large number of particles is launched with the initial propagation direction $\hat{\boldsymbol{s}}'_{init} = (1,0,0)^T$ at the origin of a Cartesian reference system x'_1-x'_2-x'_3. To retrieve the new position and propagation direction of a particle in a numerical light scattering simulation with homogeneous substrates from such a pre-computed table, the reference system x'_1-x'_2-x'_3 is first rotated such that the first coordinate direction becomes aligned with $\hat{\boldsymbol{s}}(t)$. Then, by a cheap and completely arbitrary table lookup, $\hat{\boldsymbol{x}}'(t+\Delta t) - \hat{\boldsymbol{x}}'(t)$ and $\hat{\boldsymbol{s}}'(t+\Delta t)$ are obtained and can be transformed into the absolute coordinate system to get $\hat{\boldsymbol{x}}(t+\Delta t)$ and $\hat{\boldsymbol{s}}(t+\Delta t)$. The new particle energy is calculated like in stochastic Monte Carlo methods, i.e. $\hat{e}_p(t+\Delta t) = e^{-c\gamma_a \Delta t}\hat{e}_p(t)$. Note that for anisotropic patches the stencil method has to be generalized by introducing individual tables for different initial directions $\hat{\boldsymbol{s}}(t)$. Moreover, in order to resolve the patch boundaries adequately, additional tables for smaller time steps are required. In this paper these issues are not further discussed and only isotropic substrate structures are considered. For a detailed description of the stencil method we refer to the literature [3, 4].

Multi-Scale Approach

While the stencil method is an efficient approach to compute $I(\boldsymbol{x},\boldsymbol{s})$ in homogeneous substrates, the time step size Δt has to be chosen such that $c\Delta t$ is small enough to properly resolve the geometry of the substrate and the various patches. This can result in extremely high computational costs. For example, large areas of halftone prints consist of a relatively thin paper substrate with a huge number of ink patches (dots). Obviously, resolving all important details would require a very large number of particles and tiny time steps.

Here, a multi-scale algorithm is devised, which allows to efficiently compute the statistics of the light reflected by and transmitted through a large halftone sample. The algorithm is based on the assumption that the sample can be represented adequately by a periodically repeating, much smaller patch. If this assumption is justified and one is only interested in the statistics of the transmitted and reflected light, the computation of the particle trajectories inside the paper can be omitted. The relevant information for a particle entering the substrate with the propagation

direction $\hat{\boldsymbol{s}}$ consists of its relative exit position $\hat{\boldsymbol{r}}'$ and its relative propagation direction $\hat{\boldsymbol{s}}'$ as well as the times T_{paper} and T_{dot} spent within the substrate and the dots, respectively (see Fig. 7). To obtain the required statistics, an a-priory Monte Carlo simulation of a diffuse light source illuminating a small, but representative halftone patch is performed. Fig. 3 shows the homogeneous isotropic light source at the top of the rectangular computational domain with periodic boundary conditions at the side walls. An example of a remission intensity pattern is shown in Fig. 4, where the optical dot-gain effect can be observed.

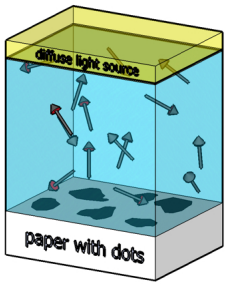

Figure 3. *Simulation setup for the multi-scale table generation.*

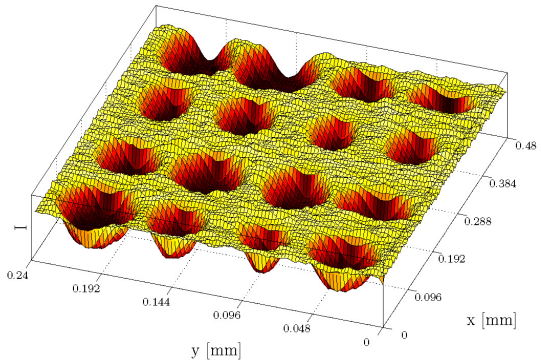

Figure 4. *Remission intensity at the paper surface with a statistically representative dot pattern illuminated by a diffuse light source.*

For this pre-processing step, the stencil method can be employed to further improve the computational efficiency. Moreover, surface effects are accounted for by reflecting a particle with a probability consistent with Fresnel's law [11]. Therefore, a thin surface layer with a somewhat higher refractive index than that of air (the refractive index inside the paper is assumed to be the same as of air) is considered (see Fig. 5). At this point, a perfectly smooth planar surface is assumed. It is possible, however, to account for more realistic surface normal direction distributions.

For each particle entering the paper, a new entry is created in a multi-scale table corresponding to the incident angle $\alpha = \arccos(\boldsymbol{n} \cdot \hat{\boldsymbol{s}})$, where $\boldsymbol{n}$ is the unit normal vector at the paper surface. The entry contains the relative separation vector $\boldsymbol{r}' = ((\hat{\boldsymbol{x}}^{out} - \hat{\boldsymbol{x}}^{in}) \cdot \boldsymbol{e}'_1, (\hat{\boldsymbol{x}}^{out} - \hat{\boldsymbol{x}}^{in}) \cdot \boldsymbol{e}'_2, 0)^T$, the new relative propagation direction $\hat{\boldsymbol{s}}' = (\hat{\boldsymbol{s}}^{out} \cdot \boldsymbol{e}'_1, \hat{\boldsymbol{s}}^{out} \cdot \boldsymbol{e}'_2, \hat{\boldsymbol{s}}^{out} \cdot \boldsymbol{n})^T$, the time $T_{paper} - T_{dot}$ spent inside the uncolored paper and the time T_{dot} spent inside the colored paper. The unit vectors $\boldsymbol{e}'_1 = (\hat{s}_1, \hat{s}_2, 0)^T / (\hat{s}_1^2 + \hat{s}_2^2)^{0.5}$ and $\boldsymbol{e}'_2 = \boldsymbol{n} \times \boldsymbol{e}'_1$ are aligned with the first and second coordinate directions of the local system. Obviously, the size of the multi-scale tables grows, i.e. the statistics improves, the longer the pre-processing simulation lasts. Note

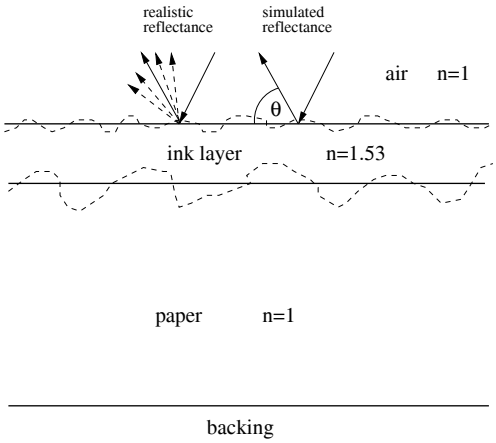

Figure 5. *Numerical modeling of surface reflectance effects.*

that in this form the algorithm relies on the assumption that the halftone print is homogeneous and isotropic. Extensions, which would require more tables, are not discussed in this paper.

For the specific light scattering simulations involving large, homogeneous and possibly geometrically complex halftone surfaces, particles are tracked until their paths intersect with a surface. To obtain the new state of a particle hitting the surface at $\hat{\boldsymbol{x}}^{in}$ with propagation direction $\hat{\boldsymbol{s}}^{in}$, an arbitrary entry $\{\hat{\boldsymbol{r}}', \hat{\boldsymbol{s}}', T_{paper}, T_{dot}\}$ from the multi-scale table corresponding to the incident angle $\alpha = \arccos(\boldsymbol{n}^{in} \cdot \hat{\boldsymbol{s}}^{in})$ is selected. For the duration T_{paper} the particle falls asleep, before it awakes at the new position $\hat{\boldsymbol{x}}^{out} = \hat{\boldsymbol{x}}^{in} + \hat{r}'_1 \boldsymbol{e}'_1 + \hat{r}'_2 \boldsymbol{e}'_2 + \hat{r}'_3 \boldsymbol{e}'_3$ with the new propagation direction $\hat{\boldsymbol{s}}^{out} = \hat{s}'_1 \boldsymbol{e}'_1 + \hat{s}'_2 \boldsymbol{e}'_2 + \hat{s}'_3 \boldsymbol{e}'_3$. Again, $\boldsymbol{e}'_1 = (\hat{s}_1^{in}, \hat{s}_2^{in}, 0)^T / (\hat{s}_1^{in^2} + \hat{s}_2^{in^2})^{0.5}$, $\boldsymbol{e}'_2 = \boldsymbol{n} \times \boldsymbol{e}'_1$ and $\boldsymbol{e}'_3 = \boldsymbol{n}$ are the unit coordinate vectors of the local system.

The particle's new energy becomes $\hat{e}_p^{out} = \hat{e}_p^{in} e^{-cT_{dot}\gamma_{a_{dot}} - c(T_{paper} - T_{dot})\gamma_{a_{paper}}}$, where $\gamma_{a_{dot}}$ and $\gamma_{a_{paper}}$ are the absorption coefficients of the colored and uncolored paper, respectively. Note that these absorption coefficients vary for different paper and ink and depend on the wavelength. Still, the reflected and transmitted intensities can be computed for different light spectra and for different dot colors without redoing the simulation, if one can neglect the wavelength dependence of the phase function, the surface reflectance and the scattering coefficient. As an example, Fig. 6 shows the

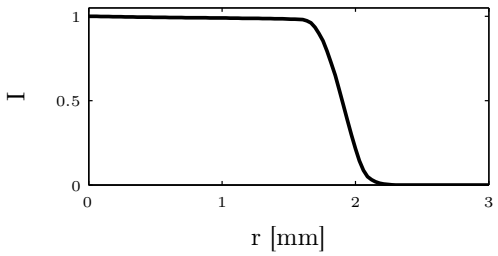

Figure 6. *Normalized radial intensity profile of the light remitted from the upper paper surface and detected by the sensor's aperture.*

computed distribution of the captured intensity from the paper surface in an i1 device as a function of the radial distance from the symmetry axis.

Simulation of Colorimetric Measurements

Generally, colorimetric assessments are based on reflectance measurements of small uniform color patches. In our

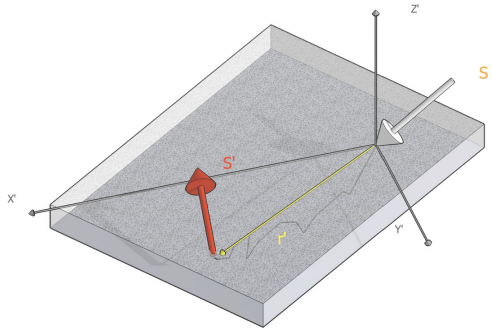

Figure 7. *Graphical representation of a multi-scale table entry.*

considerations, *reflection* defines the process of optical radiation being returned by a given medium without any change in wavelength. *Reflectance* is the ratio of reflected to incident radiation flux. The term *factor* is used when the collected radiation lies within an isolated geometric cone of the covering hemisphere [10]. From the *spectral* perspective, the visible region of radiation is sampled at consecutive wavelength bandwidths $\Delta\lambda_i$. These bandwidths are determined by the used *monochromator* with its application geometry and need not to be equally broad over the sampled spectrum.

By definition, the reflectance factor is the ratio of the radiant flux actually reflected by a sample surface to that which would be reflected into the same reflected-beam geometry by an ideal (lossless) perfectly diffuse (lambertian) standard surface irradiated in exactly the same way as the sample [9]. Most common reflectometers or spectrophotometers use a $(45/0^\circ)$ - observing condition as recommended by CIE. Usually, the illumination unit of typical hand-held instruments consists of a cone-shaped glass illuminated by up to three different unpolarized light sources. This setup produces a fairly uniform conical illumination condition, which helps to simplify the radiometric relations and to diminish the measurement dependencies on the sample orientation. In order to refer to both geometries of illumination and observation, the term *biconical* is introduced. In detail, the colorimetric quantity of interest is called the *biconical spectral reflectance factor* or short *reflectance* $R(\lambda)$ [9]. In accordance with the conservation of energy, reflectance is expressed either as percentage $(0-100\%)$ or as a factor $(0.0-1.0)$. A reproducibility of $\pm 0.5-1\%$ in the reflectance is considered sufficient for most applications.

The irradiance incident on the sample $I_0(\lambda)$ while measuring is unknown. Hence, and in accordance to its definition above, the reflectance $R(\lambda)$ is proportional to the readout of the object's returned radiance $I(\lambda)$ relative to the readout $I_D(\lambda)$ from an identically illuminated *perfectly reflecting diffuser*. Since the intensity of the light source varies additionally over the life time of the source, the above definition implies having such a diffuser available at hand with a constant reflectance distribution over the considered beam geometries. In practice, the perfectly reflecting diffuser is replaced, however, by a calibrated *white standard* consisting e.g. of a coated and painted metallic plate. Its traceable reflectance $R_D(\lambda)$ allows to determine the spectral *calibration factor* $C(\lambda)$ required to scale the spectral readouts, which is usually done automatically by the instrument after calibration. Accordingly, in order to compare our calculations with measurements, we transform our radiance calculations $I(\lambda)$ into predictions of reflectance measurements $R(\lambda)$ using the scaling equation

$$R(\lambda) = \frac{\pi}{\Omega_i \Omega_r} C(\lambda) I(\lambda) \tag{4}$$

with the calibration scaling factor $C(\lambda) = R_D(\lambda)/I_D(\lambda)$ and the solid angles of incidence and reflection, Ω_i and Ω_r, respectively. Obviously, in a standard simulation setup, the calibration factor $C(\lambda)$ equals to the reciprocal of the number of simulation particles incident on the sample.

Results

Here, it is demonstrated that our simulation framework is capable of capturing the different device geometries and can properly account for the optical characteristics of the employed paper substrate. Therefore, comparative macroscopic and microscopic studies of the reflectance spectra from halftone and solid patches printed on sheet feed offset papers with an average thickness of 0.142mm were performed. First, the illumination and capturing geometries of the employed instruments, i.e. an i1 device and a combination of a high-end Leica microscope with spectrophotometer, were determined. A sketch of the geometry representative for both devices is depicted in Fig. 2 and Table 1 shows the individual geometrical parameters. At the top of Fig. 2 one can see the ring-shaped light source with the detector at the center, and at the bottom one finds the paper as a light scattering substrate. The arrows indicate incident (white), reflected (gray and red) and gonna-be-detected (red) particles. At this point, only unpolarized light is considered.

Table 1: Geometry parameters of both instruments according to Fig. 2 (all in *mm*).

instrument	*a*	*b*	*c*	*d*	*e*	*f*
i1	6	3.5	2.15	2.35	5.7	5.7
microscope	7	3	1.125	1	4.5	2.55

Model Calibration

In order to determine the paper's optical characteristics, the paper was simply modeled as a scattering and absorbing bulk with a refractive index of 1 covered by an ink/coating layer with a refractive index of 1.53 [5] (see Fig. 5). Based on a microscopic section analyses of the printed paper (as proposed in [6]), the average ink penetration depth was determined to be approximatively 10% of the paper thickness.

To estimate the relevant optical parameters, the absorption and scattering cross sections were calibrated based on microscopic measurements using the method presented in [7]. By assuming a non-scattering ink layer and by fixing the refractive indices, the number of required degrees of freedom for the optimization process could be reduced from eight to three. To estimate the absorption and scattering coefficients, two reflectance measurements of the pure paper without ink on black and white backings were performed. The obtained coefficients of the pure paper are kept constant during the subsequent simulation with uniform ink coating to estimate the ink absorption coefficient. These three calibration simulations are also based on reflectance measurements of the black and white backings, for which the microscope setup was used. With this calibration procedure based on solid patches it was possible to determine the required optical coefficients for computational investigations of halftone patches with different ink coverage.

Prediction Results

The set of derived absorption and scattering coefficients was used together with the multi-scale simulation framework to predict i1 reflectance measurements. Therefore, pure paper with-

out ink and magenta halftone patches with different ink coverage were considered. In all cases a black backing was employed. To characterize the dot patterns of representative, periodically repeating patches required for the simulations to generate the multi-scale tables, the average dot diameters and the dot density was determined with the microscope. To account for the different halftone samples, only the dot diameters were varied. For the simulations, simplified cylindrical dot shapes with a penetration depth equal to 10% of the paper thickness were used. For the reflectance studies presented here, the influence of possible brightening additives in the paper [8] was avoided and only two wavelengths of 550nm and 580nm were considered (see Fig. 1).

As shown in Figs. 8, 9, 10 and 11 the computational predictions demonstrate reasonable agreement with the corresponding measurements for both devices and for the whole ink coverage range.

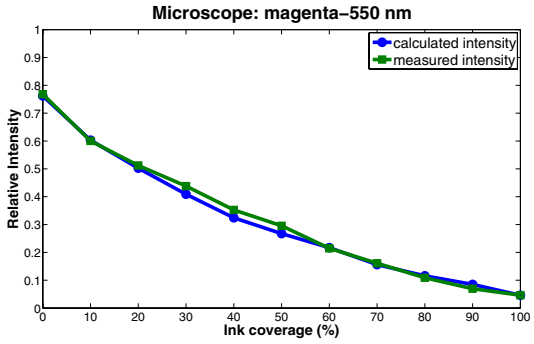

Figure 8. *Numerical predictions and measurements for the microscope setup.*

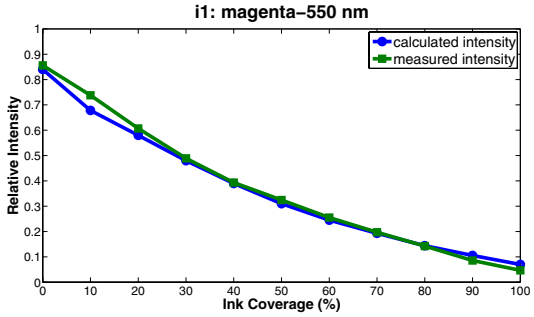

Figure 9. *Numerical predictions and measurements for the i1 device.*

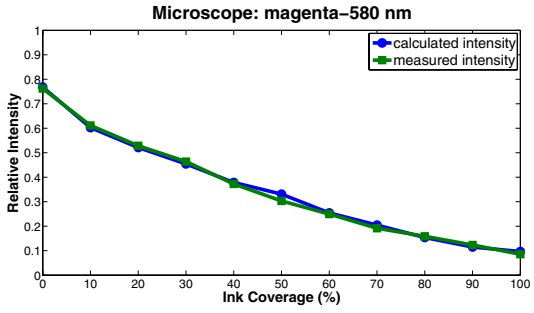

Figure 10. *Numerical predictions and measurements for the microscope setup.*

The results in figure Fig. 12 demonstrate the influence of the scattering coefficients on the numerical predictions. Increasing the scattering coefficient by a factor of ten results in a higher

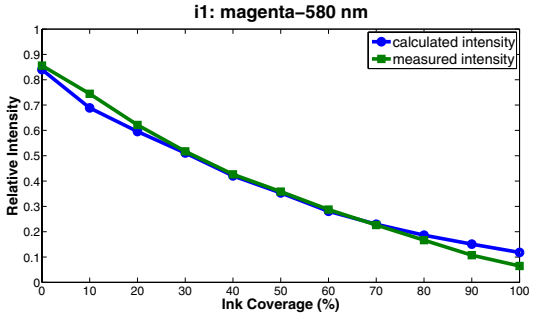

Figure 11. *Numerical predictions and measurements for the i1 device.*

reflectance with hardly any dot gain, i.e. the measured intensity is almost a linear function of the ink coverage (upper dashed, red curve. A ten times lower scattering coefficient, on the other hand, leads to a weaker reflectance (lower dashed, cyan curve).

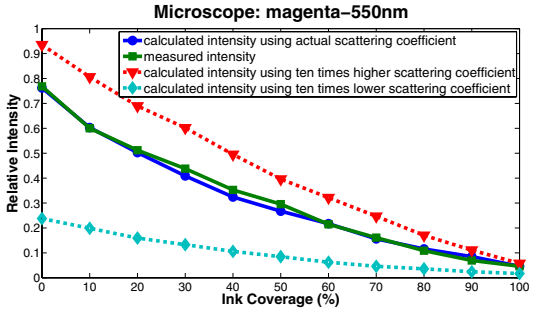

Figure 12. *Comparison between the measurements and the numerical results with different scattering coefficients.*

Conclusion

A new Monte Carlo based multi-scale method for light scattering simulations with large, homogeneous halftone patches is devised. The algorithm is very efficient and current results are in excellent agreement with the corresponding measurements. This is promising for future predictions of device dependent measurements, e.g. the multi-scale algorithm allows to predict the correct optical dot gain and geometry induced deviations between different spectral measuring devices. Eventually, this capability will allow us to convert the results from one device to another. In its current form, the multi-scale algorithm can be employed to investigate isotropic dot patterns only. Moreover, realistic paper surface normal distributions are not implemented yet and no fluorescence effects are considered. Corresponding extensions are planned in the near future.

Acknowledgments

This project was partly supported by the Swiss Innovation Promotion Agency (grant KTI/CTI 8804.1 PFES-ES).

References

[1] A. Ishimaru. *Wave Propagation and Scattering in Random Media*, volume I & II. Academic Press, 1978.

[2] L. Wang, J. L. Jacques, and L. Zheng. MCML - monte carlo modeling of photon transport in multi-layered tissues. *Computer Methods and Programs in Biomedicine*, 47:131–146, 1995.

[3] P. Jenny, M. Vöge, S. Mourad, and T. Stamm. Modeling light scattering in paper for halftone print. In *Proc. CGIV*, pages 443–447. IS&T, 2006.

[4] P. Jenny, S. Mourad, T. Stamm, M. Vöge, and K. Simon. Computing

light statistics in heterogeneous media based on a mass weighted probability density function method. *Journal of the Optical Society of America, A.*, 24(8):2206–2219, August 2007.

[5] R. D. Hersch, P. Emmel, F. Collaud, and F. Crété. Spectral reflection and dot surface prediction models for color halftone prints. *Journal of Electronic Imaging*, 14(3), Jul-Sep 2005.

[6] L. Yang, A. Fogden, N. Pauler, Ö. Sävborg, and B. Kruse. A novel method for studying ink penetration of a print. *Nodic Pulp and Paper Research Journal*, 20:423–429, 2005.

[7] S. Mourad. Improved calibration of optical characteristics of paper by an adapted paper-MTF model. *Journal of Imaging Science and Technology*, 51(4):283–292, July/August 2007.

[8] S. Mourad. Color predicting model for electrophotographic prints on common office paper. *École Polytechnique Fédérale de Lausanne*, PhD thesis No 2708, February 2003.

[9] F. E. Nicodemus, J. C. Richmond, J. J. Hsia, I. W. Ginsberg, and T. Limperis. Geometrical considerations and nomenclature for reflectance. Monograph NBS MN-160, National Bureau of Standards (US), October 1977.

[10] R. W. G. Hunt. *Measuring Color*. Fountain Press, 3rd edition, 1998.

[11] G. Wyszecki and W. S. Stiles. *Color Science: Concepts and Methods, Quantitative Data and Formulae*. John Wiley & Sons, Inc., 2nd edition, 1982.

Author Biography

Milos Sormaz, graduated in 2003 as a mechanical engineer from the University of Split, Croatia. From 2006 to 2007 he worked with Alstom Power in Switzerland as a structural engineer. Since 1.May 2007 he joined the Institute of Fluid Dynamics, ETH Zurich, as a PhD student currently working on numerical predictions of light scattering within the paper substrate.